Simulation study of second-harmonic microscopic imaging signals through tissue-like turbid media

Xiaoyuan Deng
Xianju Wang
Hanping Liu
Zhengfei Zhuang
Zhouyi Guo
South China Normal University
School for Information and Optoelectronic Science & Engineering
Laboratory of Photonic Chinese Medicine
Shipai, Guangzhou, China, 510631
E-mail: xiaoyuandeng@yahoo.com.cn

Abstract. We establish, for the first time, a simulation model for dealing with the second-harmonic signals under a microscope through a tissue-like turbid medium, based on the Monte Carlo method. With this model, the angle-resolved distribution and the signal level η of second-harmonic light through a slab of the turbid medium are demonstrated and the effects of the thickness (d) of the turbid medium, the numerical aperture (NA) of the objective as well as the size (ρ) of the scatterers forming the turbid medium are explored. Simulation results reveal that the use of a small objective NA results in a narrow angle distribution but strong second-harmonic signals. A turbid medium consisting of large scattering particles has a strong influence on the angle distribution and the signal level η, which results in a low penetration limit for second-harmonic signals made up of ballistic photons. It is approximately 30 μm in our situation. [DOI: 10.1117/1.2191055]

Keywords: second-harmonic generation; multiple scattering; multiphoton processes; nonlinear optics; microscopy; simulations.

Paper 05238R received Aug. 17, 2005; revised manuscript received Nov. 15, 2005; accepted for publication Nov. 18, 2005; published online Apr. 17, 2006.

1 Introduction

Nonlinear optics has been proved to be a powerful tool for biomedical studies.[1] Since its first demonstration by Denk et al.[2] in 1990, two-photon fluorescence microscopic imaging has been widely applied to a variety of biological imaging tasks in aspects of physiology, morphology, and cell-cell interactions, etc.[1–3] More recently, nonlinear microscopies based on radiative second-harmonic generation (SHG) have dramatically emerged as a viable microscope imaging contrast mechanism for visualization of cell and tissue structures and functions.[4–9]

The nonlinear optical effect known as SHG was recognized in the earliest days of laser physics. Two decades ago, it was successfully demonstrated through a microscope by Gannaway and Sheppard[10] and was first applied[11] in biological tissue in 1986. SHG is commonly called frequency doubling and the second-harmonic light emerging from the material is at precisely half the wavelength of the light entering the material.

SHG has been widely investigated both experimentally and theoretically. Second-harmonic signals from collagen fibrils have been quantitatively explored based on theoretical physical models[12–14] and the biophysical features characteristic of collagen structures can be resolved from the experimental second-harmonic microscopic images on the basis of the SHG phase-matching fundamental principles.[15] SHG from both single and arrays of spherical particles have been theoretically explored or experimentally observed.[16–20] Meanwhile, the second-harmonic (SH) cross section, as well as the average cosine of the SH scattering angle is theoretically calculated in a dilute suspension of spherical particles confined within a very thin slab[21] (the thickness of the slab $d \ll$ the scattering length l of the turbid medium). The angle-resolved pattern of the SH light scattering from suspensions of different sizes of centrosymmetric microsize polystyrene spheres with surface-absorbed dye (malachite green) has been experimentally measured.[22] However, as we have noticed, all the researchers have focused on the generation mechanism study of SH signals in either an isolate or a suspension of particles. The scattering effect of the turbid medium itself in which the SH signals generate and go through has not been paid much more attention. As our intension is directed to the SH microscopic imaging studies in the biological tissue, a kind of highly scattered media, the studies of the SH signals through a turbid medium becomes absolutely necessary.

Because biological tissue is usually composed of scatters with a size variation from nanometers to a few micrometers,[23] the dominant effect caused by these scatterers is Mie scattering. To understand the effect of multiple scattering in multiphoton fluorescence microscopy, one usually uses the Monte Carlo simulation method based on Mie scattering because the conventional image theory based on Fourier optics is not applicable.[24–26] So far the established Monte Carlo method in multiphoton microscopy is in fluorescence applications.[27–29] This paper establishes a Monte Carlo simulation model for SH microscopic imaging through turbid media.

The paper is organized as follows. Section 2 describes the simulation model of the SH microscopic imaging through a turbid medium. In Sec. 3, we demonstrate the simulation re-

Address all correspondence to Xiaoyuan Deng, School for Information and Optoelectronic Science and Engineering, South China Normal University, Shipai, Guangzhou 510631 China. Tel: 86–20–3353 0799, Fax: 86–20–8521 0889. E-mail: xiaoyuandeng@yahoo.com.cn

1083-3668/2006/11(2)/024013/6/$22.00 © 2006 SPIE

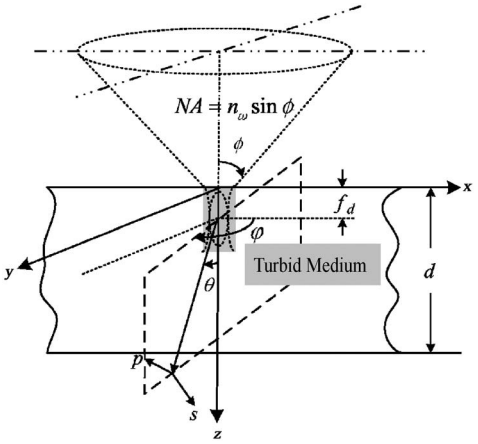

Fig. 1 Schematic diagram of imaging through a turbid medium in a transmission-mode SH microscope, where f_d is the focal depth, and d is the thickness of the turbid medium. The coordinate system defining the SHG emission direction is also shown. The shaded part demonstrates the membrane surface, which can be approximated to be planar at the length scales considered. The focused excitation beam propagates in the $+z$ direction. The resultant SHG signal is mostly confined to an interaction area schematically depicted as a dotted ellipsoid and radiates in the directions defined by θ and φ.

sults of the angle-resolved SH signal distribution and the signal level η under different constraints of the scattered numbers (n_s). The effect of the parameters such as the thickness d of the turbid media, the numerical aperture (NA) of the objective, and the particles size (ρ) that form the turbid medium are investigated. Discussion and conclusions are presented in Sec. 4.

2 Simulation Model for SH Microscopic Imaging through a Turbid Medium

Figure 1 shows the schematic diagram for SH microscopic imaging through turbid media in a transmission mode. It is supposed that the excitation light is focused through an imaging objective with NA$=n_\omega \sin\phi$ on to a focal plane. An SH signal of a certain strength and direction within the focal spot are generated and then propagate through a thickness d in the turbid medium. The focal depth f_d is the distance between the turbid medium's surface and the focal plane. In this paper, we choose $f_d \approx 0$ (imaging near the surface) to avoid the influence coming from the polarization change of the excitation light due to scattering. The turbid medium is supposed to be a slab formed by microsize scattering particles (ρ).

The Monte Carlo simulation method for multiphoton fluorescence microscopic imaging through the turbid medium is adopted and the basic principle is the same as that described elsewhere.[27–29] However, for SH microscopic imaging, the implementation is much more complicated than that in fluorescence imaging. Unlike the process of two-photon-excited fluorescence (TPF), an SHG process is a coherent scattering process, in which the scattered photons must satisfy a phase-matching constraint, and thus produces highly directed radiation rather than isotropic emission.

According to a simplified biophysical model, the total power distribution of SHG emitted from the cell membrane labeled by Di-6ASPBS styryl dye is (the details can be found in the Appendix[30]):

$$P_{\mathrm{SHG}}(\theta,\varphi) = 1/2\Theta_y(\theta,\varphi)N^2\sigma_{\mathrm{SHG}}I_\omega^2.$$

Therefore, three steps are involved to implement it. First, the average photon intensity distribution $\langle I_\omega \rangle$ at focal depth f_d is calculated using the Monte Carlo simulation. Since in this paper, it is supposed that a pulse laser with pulse duration $\tau = 100$ fs and a repetition frequency of $R = 80$ MHz is used as the excitation light to approach reality, with the pulse laser, the two-photon excitation depends on the average squared intensity $\langle I_\omega(t)^2 \rangle$ rather than the squared average intensity $\langle I_\omega(t) \rangle^2$, which yields[1]

$$\langle I_\omega(t)^2 \rangle = g_p \langle I_\omega(t) \rangle^2 / (R\tau),$$

where the dimensionless factor $g_p = 0.66$ is used for a Gaussian pulse shape.

Second, the simulation starts from the beginning. This time, for each excitation photon, a direction (θ,φ) is produced according to $\theta = \pi\zeta$, $\varphi = 2\pi\zeta$ (where ζ is a uniformly distributed random number) and SH signals will generate with the weighting factor $g_p\langle I_\omega(t) \rangle / (R\tau)$ and the efficiency factor $\alpha_{\mathrm{SHG}} = 1/2\Theta_y(\theta,\varphi)N^2\sigma_{\mathrm{SHG}}$ at that direction (θ,φ). Once it is generated, the propagation of the SH light follows the same way as that detailed in Ref. 29 for TPF.

The excitation wavelength is assumed to be 800 nm and the SH emitted is therefore assumed to be 400 nm. The excitation power after the objective is 10 mw. The collective NA of the objective in this transmission model is supposed to be always the same as that of the excitation objective. According to the Mie scattering theory,[31] the corresponding parameters of anisotropy value (g), the scattering cross section (σ_i) and the scattering mean-free-path length (l) of the scatterers (at a concentration of $0.5/\mu\mathrm{m}^3$) in the simulated turbid medium are shown in Table 1.

Table 1 Scattering parameters of the turbid medium under $2p$ excitation.

	$2p$ Excitation $\lambda_{ex} = 800$ nm			SH $\lambda_{SH} = 400$ nm		
ρ (μm)	g	σ_s (μm^2)	l (μm)	g	σ_s (μm^2)	l (μm)
0.6 (L)	0.804	0.193	10.36	0.916	0.686	2.92
0.3 (S)	0.45	0.00877	228.05	0.804	0.0483	41.41

The concentration of the molecular surface density N_s is assumed to be $10^5/\mu\mathrm{m}^2$ and the first hyperpolarizability of the dye molecule is $\beta \approx 1 \times 10^{-47}$ C m^3 V^{-2}.

Two indicators, the angle-resolved SH signal distribution on the emitted plane along the x-y direction and the signal level η collected immediately after the emitted plane, are adopted in this paper. The signal level (η) is defined as the number of SH photons collected by the detector under different maximum scattering number limits (n_s) and normalized by the number when no scattering exists (or the thickness $d \approx 0.0$ μm). Here, we should clarify that we use the limit of

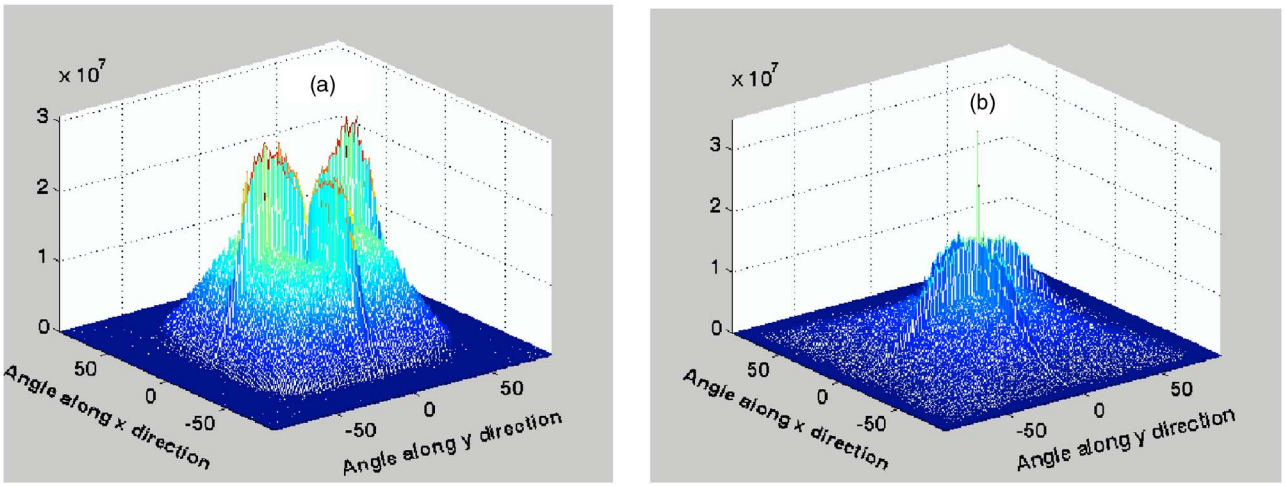

Fig. 2 Angle-resolved distributions of the SH signals under NA=1.2 in the turbid medium formed by scattering particles of a size of ρ=0.6 μm at (a) $d\approx$0.0 μm and (b) d=30.0 μm.

$n_s \leqslant 5$ to implicate that the SH signals are dominated by ballistic photons, which means the basic features of the photon, such as the polarization, the coherence, etc., are kept at a maximum degree; the limit of $n_s \leqslant 10$ includes the effect from both ballistic and snakes SH photons; while $n_s \leqslant 300$ means all the effects including the multiple scattered photons are considered.

3 Angle-Resolved SH Signals and Signal Level η through Turbid Media

3.1 *Effect of the Thickness d of the Turbid Media*

The thickness d of the turbid medium is important when we decide to explore the signal changes through a turbid medium as it directly influences the number of the scattering events, thus inducing the direction change of the photons and the collection efficiency. Therefore, in this paper, the effect of the thickness d is first investigated.

Figures 2(a) and 2(b) show the angle-resolved distributions of the total SH signals ($n_s \leqslant 300$) under NA=1.2 in a turbid medium formed by the scattering particle size of ρ=0.6 μm under $d\approx$0.0 μm and d=30.0 μm, respectively. From the comparison of the Figs. 2(a) and 2(b), we can see that as the d increases, the angle distribution of the SH signals becomes disperse along both the x and y directions. However, the lobe effect induced by the Gouy shift[31] becomes unobvious because of the multiple scattering.

Figure 3 shows the change of the signal level η as the increase of the thickness d under different maximum scattering number limits (n_s), respectively. It is shown that as the d increases, the collected SH signals decrease under all three conditions. In practice, we are much more interested in the SH signals that are composed of ballistic photons (the solid line in Fig. 3 presents for the ballistic SH signal level η versus d), since the fewer scattering events they experience, the less carried information they lose. It is shown that as the thickness d reaches 30 μm, the SH signals made up of ballistic photons almost disappear. In another words, the penetration limit of ballistic SH signals is 30 μm under the condition described. After an approximate penetration depth of 10 μm, the signal level η drops to half the height of the total signals.

3.2 *Effect of the Objective NA*

The size of the objective NA is proved to play a role in multiphoton fluorescence microscopic imaging.[32] In this paper, its effect on the SH microscopic imaging is thus investigated.

Figures 4(a) and 4(b) demonstrate the angle distribution of the total collected SH signal ($n_s \leqslant 300$) under NA=0.6 under thicknesses $d\approx$0.0 μm and d=30.0 μm, respectively. It is clear from a comparison of Fig. 4 with Fig. 2 that NA has a significant effect on both the angle distribution and the signal strength of SH signals. As NA becomes smaller, the angle distribution becomes narrower, while many more SH signals are collected. According to a relationship[31] of $\theta_{\text{peak}}/\theta_{\text{NA}}$ to NA, where $\theta_{\text{NA}}=\sin^{-1}(\text{NA}/n_\omega)$, in our situation, when NA =1.2 and NA=0.6 are used, the peak angle of the lobes of SH emission will locate at $\theta_{\text{peak}}\approx 50$ deg and $\varphi\approx\pi/2$ and $\theta_{\text{peak}}\approx 20$ deg and $\varphi\approx\pi/2$, respectively. This provides the

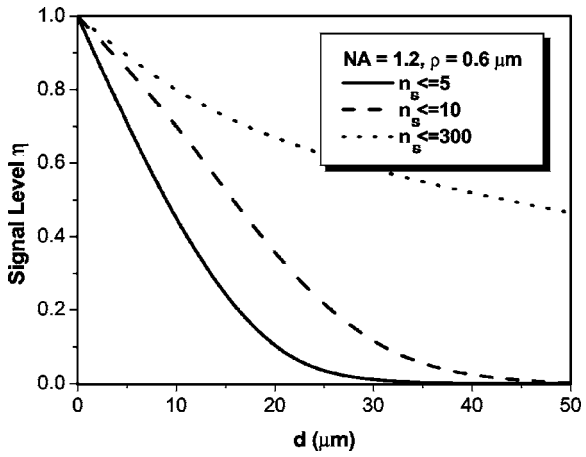

Fig. 3 Signal level η of the SH signals under NA=1.2 in the turbid medium formed by the scattering particles with size of ρ=0.6 μm along the thickness d of the turbid medium.

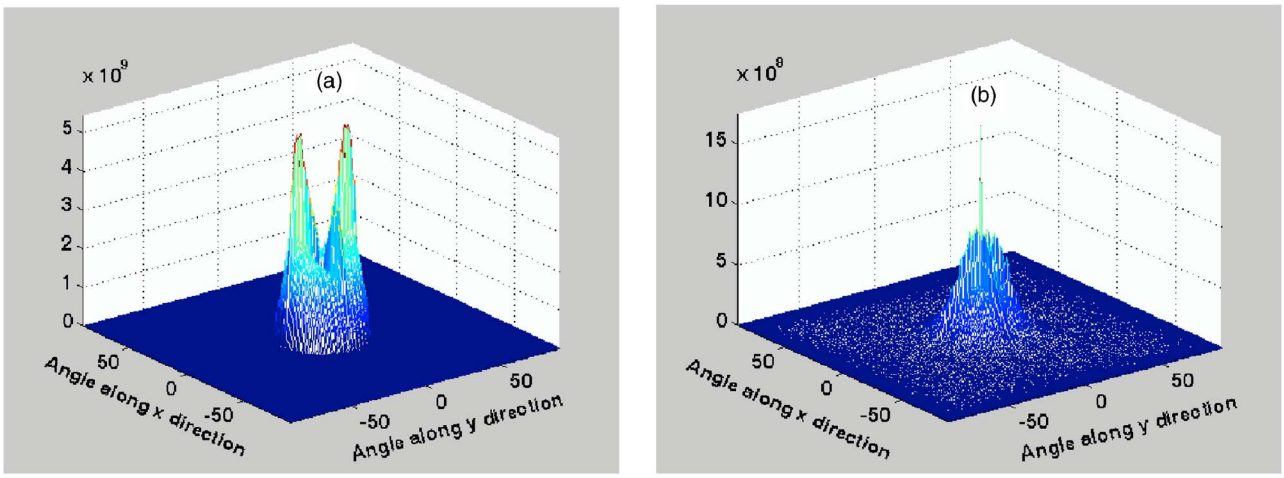

Fig. 4 Angle-resolved distributions of the SH signals under NA=0.6 in the turbid medium formed by scattering particles of a size of ρ=0.6 μm at (a) $d \approx 0.0$ μm and (b) d=30.0 μm.

explanation for why at a low NA, the distribution of the ballistic SH signals are narrow (Fig. 4). Meanwhile, because ω_z and ω_x are[1] inversely proportional to NA, as the NA becomes low, the effective total number of molecules $N=(\pi/2)\omega_z\omega_x N_s$ that contribute to the generation of SH light becomes large. Therefore, the power of SH light becomes strong (Fig. 4). Figure 5 shows the corresponding signal level η versus d under three scattering number constraints. We notice that NA has no obvious effect on the penetration limit regarding the ballistic SH signals if the same turbid medium is provided (see solid lines in Figs. 3 and 5). However, it does influence the collected snake and multiple scattered SH signals, which can be realized from a comparison of the dotted and the dashed lines in Figs. 3 and 5. For a small NA (Fig. 5), the collected snake and multiple scattered SH signals have a greater rate of decrease as d increases than that for a large NA, which means a small NA has a suppression function to snake and multiple scattered SH signals.

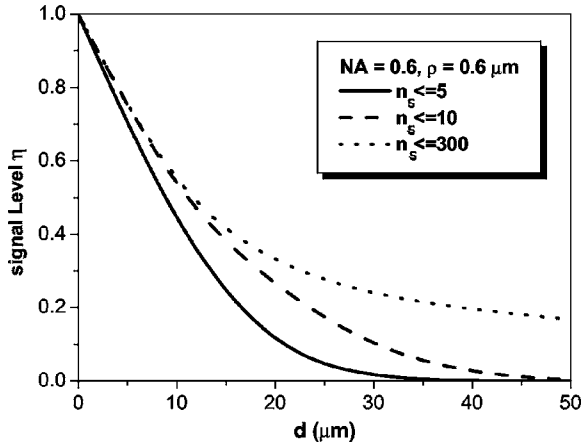

Fig. 5 Signal level η of the SH signals under NA=0.6 in the turbid medium formed by the scattering particles with a size of ρ=0.6 μm along the thickness d of the turbid medium.

3.3 *Size Effect of the Spherical Particles (ρ) in the Turbid Medium*

The size effect of the spherical particles ρ that form the turbid medium is also part our investigation scope in this paper, since different scatterer sizes have different scattering cross sections (σ_s) and anisotropy values (g) according to Mie scattering, which may directly influence the behavior of SH light during the turbid medium. In this paper, two sizes of particles are chosen as our objects. One is the larger one (L) with a diameter of 0.6 μm and the other is the smaller one (S) with a diameter of 0.3 μm.

Figures 6(a) and 6(b) demonstrate the total angle-distribution of SH signals ($n_s \leqslant 300$) under thicknesses of $d \approx 0.0$ μm and d=30.0 μm, respectively. It is shown that the angle-distribution has no obvious difference under thicknesses of d=30.0 μm compared with that for $d \approx 0.0$ μm. Figure 7 is the signal level η versus d under three scattering number (n_s) constraints. We noticed that the signal level η under three scattering number (n_s) constraints also has a slight difference along the whole thickness d and the drop of the signal level η is very low. This is because the small scattering particles have a much smaller cross section (σ_s) than that of large particles (Table 1). Under the same concentration, the mean-free path length (l) is much longer than that of large particles, which leads to fewer scattering events at a given thickness d. Thus, the penetration limit is much deeper than that in turbid medium with large scattering particles.

4 Discussion and Conclusion

The fluorescence signals to the excitation intensity I_ω have the relationship of $p_n=\alpha_n I_\omega^n$ (n=1,2,3 corresponding to 1p, 2p, and 3p excitation). In our previous investigation, the model of multiphoton fluorescence microscopic imaging through the turbid medium based on the Monte Carlo simulation method was successfully established,[27–29] where fluorescence photons are generated by a uniform random generator with the weighting factor of I_ω and the fluorescence efficiency factor α_n. In the case of an SH microscopic imaging condition, the phase

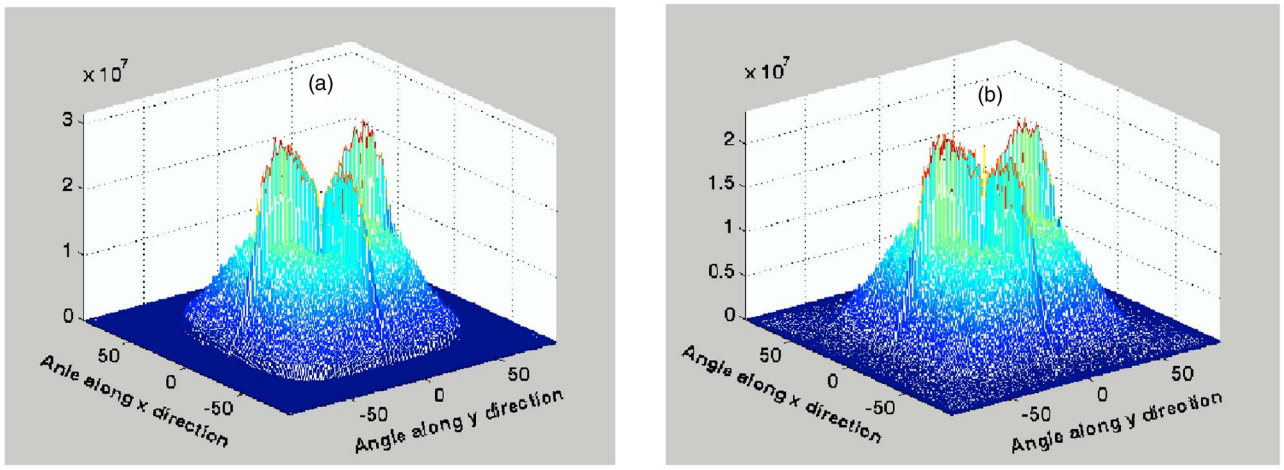

Fig. 6 Angle-resolved distributions of the SH signals under NA=1.2 in the turbid medium formed by scattering particles of a size of ρ=0.3 μm at (a) $d \approx 0.0$ μm and (b) d=30.0 μm.

matching between the SHG and the excitation fields largely prevents SHG propagation from the forward direction, and forces it to propagate off-axis to form two well-defined lobes. In this case, the SH photons generated are no longer as uniformly randomized as these of fluorescence photons, instead, the probability of the generation of the SH photons in each direction are determined based[31] on the angular structure parameter $\Theta_y(\theta,\varphi)$. Therefore, $\alpha_{\mathrm{SHG}}=0.5\Theta_y(\theta,\varphi)N^2\sigma_{\mathrm{SHG}}$ at direction (θ,φ) as the efficiency factor is implemented by Monte Carlo simulation to get the SH photons.

To efficiently demonstrate our model, in this paper, we simplified our condition of $f_d \approx 0.0$ μm. As imaging at a nonzero focal depth f_d in the turbid medium, the effect of the polarization change of the excitation beam due to the scattering must be considered. This may greatly increase the complication of the problem, and it becomes another interesting topic calling for further investigation.

To summarize, we demonstrated the simulation model based on the Monte Carlo method for dealing with SH signals through a turbid medium for the first time. The angle-resolved distribution and signal level η under various conditions were explored. Simulation results reveal that the use of the small objective NA results in a narrow angle distribution and strong SH signals. The turbid medium composed of large scattering particles has a strong influence on the angle distribution and the signal level η of SH light, which results in a low penetration limit in the turbid medium for ballistic SH signals, which is approximate 30 μm.

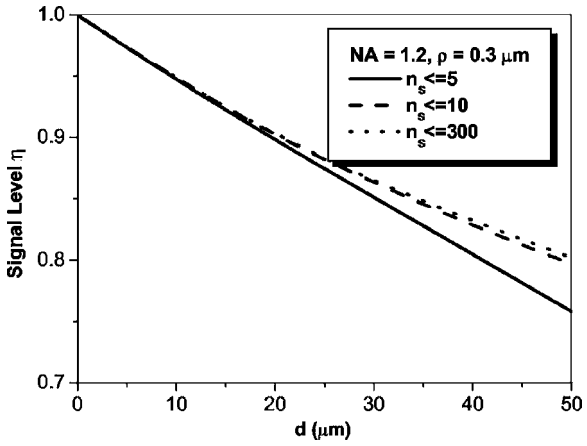

Fig. 7 Signal level η of the SH signals under NA=1.2 in the turbid medium formed by the scattering particles with a size of ρ=0.3 μm along the thickness d of the turbid medium.

5 Appendix

It is assumed that SHG is produced from Di-6ASPBS styryl dye molecules labeled on the cell's membrane surface. A tightly focused driving field under a microscope is polarized in the $\hat{y}$ direction and the molecules in the membrane are perfectly oriented in the $\hat{y}$ direction and strictly uniaxial.

Under this condition, we can assume that the amplitude of the excitation light field with frequency ω (wavelength λ) has a Gaussian profile in both the axial and the lateral directions about the focal center and that its phase near the focal center progresses linearly. That is,[30]

$$E_\omega(z,x) = -iE_\omega \exp\left(-\frac{z^2}{\omega_z^2}-\frac{x^2}{\omega_x^2}+i\xi\mathbf{k}_\omega z\right), \tag{1}$$

where $\mathbf{k}_\omega = n_\omega\omega/c$ is the local wave vector (n_ω are the indices of refraction at ω); ξ is a parameter that characterizes the phase shift, commonly referred to as a Gouy shift or a phase anomaly, experienced by a Gaussian beam in the vicinity of a focal center; and ω_z and ω_x are the axial and the radial field waists at $1/e^2$, respectively, given by[1]

$$\omega_x = \begin{cases} \dfrac{0.320\lambda}{\mathrm{NA}} & \mathrm{NA} \leqslant 0.7 \\ \dfrac{0.325\lambda}{\mathrm{NA}^{0.91}} & \mathrm{NA} > 0.7 \end{cases}$$

$$\omega_z = 0.532\lambda\left[\frac{1}{n_\omega - (\omega_\omega^2 - \mathrm{NA}^2)^{1/2}}\right]. \tag{2}$$

According to Ref. 30, the total power distribution of SHG is

$$P_{\mathrm{SHG}}(\theta,\varphi) = 0.5\Theta_y(\theta,\varphi)N^2\sigma_{\mathrm{SHG}}I_\omega^2, \tag{3}$$

where

$$\Theta_y(\theta,\varphi) = \frac{3}{8\pi}A^2(\theta,\varphi)[1-\sin^2\theta\sin^2(\varphi)]\sin\theta\Delta\theta\Delta\varphi,$$

$$A(\theta,\varphi) = \exp\left\{-\frac{\mathbf{k}_{2\omega}^2}{8}[\omega_z^2(\cos\theta-\xi n_\omega/n_{2\omega})^2 + \omega_x^2(\sin\theta\cos\varphi)^2]\right\},$$

$$N = \frac{\pi}{2}\omega_z\omega_x N_s,$$

$$\sigma_{\mathrm{SHG}} = \frac{4n_{2\omega}\hbar\omega^5}{3\pi n_\omega^2\varepsilon_0^3c^5}|\beta|^2,$$

$\mathbf{k}_{2\omega}=2n_{2\omega}\omega/c$ is the second-harmonic wave vector, I_ω is the excitation intensity in units of photons per second per area, N_s is the molecular surface density, $n_{2\omega}$ are the indices of refraction at 2ω, $\hbar$ is Planck's constant, and β denotes the first hyperpolarizability of the dye molecular.

Acknowledgment

The authors gratefully thank the National natural Science Foundation of China (Grant No. 30470495) for its support and the authors also thank Prof. Min Gu of the Centre for Microphotonics, Swinburne University of Technology, for his kind help in modification.

References

1. W. R. Zipfel, R. M. Williams, and W. W. Webb, "Nonlinear magic: multiphoton microscopy in the biosciences," *Nat. Biotechnol.* **21**, 1369–1377 (2003).
2. W. Denk, J. H. Stricker, and W. W. Webb, "Two-photon laser scanning fluorescence microscopy," *Science* **248**, 73–76 (1990).
3. K. König, "Multiphoton microscopy in life sciences," *J. Microsc.* **200**, 83–104 (2000).
4. X. Deng, E. D. Williams, E. W. Thompson, X. Gan, and M. Gu, "Second-harmonic generation from biological tissues: effect of excitation wavelength," *Scanning* **24**, 175–178 (2002).
5. P. J. Campagnola and L. M. Loew, "Second-harmonic imaging microscopy for visualizing biomolecular arrays in cells, tissues and organisms," *Nat. Biotechnol.* **21**, 1356–1360 (2003).
6. A. Zoumi, A. Yeh, and B. J. Tromberg, "Imaging cells and extracellular matrix in vivo by using second-harmonic generation and two-photon excited fluorescence," *Proc. Natl. Acad. Sci. U.S.A.* **99**, 11014–11019 (2002).
7. E. Brown, T. Mckee, et al., "Dynamic imaging of collagen and its modulation in tumors in vivo using second-harmonic generation," *Nature Med.* **9**, 796–800 (2003).
8. D. A. Dombeck, W. W. Webb, et al., "Uniform polarity microtubule assemblies imaged in native brain tissue by second-harmonic generation microscopy," *Proc. Natl. Acad. Sci. U.S.A.* **100**, 7081–7086 (2003).
9. P. J. Capagnola, W. A. Mohler, et al., "Three-dimensional high-resolution second-harmonic generation imaging of endogenous structural proteins in biological tissues," *Biophys. J.* **81**, 493–508 (2002).
10. J. N. Gannaway and C. J. R. Sheppard, "Second-harmonic imaging in the optical scanning microscope," *Opt. Quantum Electron.* **10**, 435–439 (1978).
11. I. Freund and M. Deutsch, "2nd-harmonic microscopy of biological tissue," *Opt. Lett.* **11**, 94–96 (1986).
12. P. Stoller, A. M. Rubenchik, et al., "Quantitative second-harmonic generation microscopy in collagen," *Appl. Opt.* **42**, 5209–5219 (2003).
13. P. Stoller, A. M. Rubenchik, et al., "Polarization-modulated second-harmonic generation in collagen," *Biophys. J.* **82**, 3330–3342 (2002).
14. P. Stoller and L. B. Da Silva, "Polarization-dependent optical second-harmonic imaging of a rat-tail tendon," *J. Biomed. Opt.* **7**, 205–214 (2002).
15. R. M. Williams, W. R. Zipfel, and W. W. Webb, "Interpreting second-harmonic generation images of collagen I fibrils," *Biophys. J.* **88**, 1377–1386 (2005).
16. V. L. Brudny, B. S. Mendoza, and W. L. Mochán, "Second-harmonic generation from spherical particles," *Phys. Rev. B* **62**, 11152–11162 (2000).
17. J. I. Dadap, J. Shan, K. B. Eisenthal, and T. F. Heinz, "Second-harmonic Rayleigh scattering from a sphere of centrosymmetric material," **83**, 4045–4048 (1999).
18. N. Yang, W. E. Angerer, and A. G. Yodh, "Second-harmonic microscopy of single micrometer-size particles on a substrate," *Phys. Rev. A* **64**, 045801 (2001).
19. J. I. Dadap, J. Shan, and T. F. Heinz, "Theory of optical second-harmonic generation from a sphere of centrosymmetric material: small-particle limit," *J. Opt. Soc. Am. B* **21**, 1328–1347 (2004).
20. W. Luis Mochán, J. A. Maytorena, B. S. Mendoza, and V. L. Brudny, "Second harmonic generation in arrays of spherical particles," *Reys. Rev. B.* **68**, 085318 (2003).
21. E. V. Makeev and S. E. Skipetrov, "Second-harmonic generation in suspensions of spherical particles," *Opt. Commun.* **224**, 139–147 (2003).
22. N. Yang, W. E. Angerer, and A. G. Yodh, "Angle-resolved second-harmonic light scattering from colloidal particles," *Phys. Rev. Lett.* **87**, 103902 (2001).
23. A. G. Loewy and P. Siekevitz, *Cell Structure and Function*, 2nd ed., Holt, New York (1971).
24. L. H. Wang and G. Liang, "Absorption distribution of an optical beam focused into a turbid medium," *Appl. Opt.* **38**, 4951–4958 (1999).
25. C. M. Blanca and C. Saloma, "Monte Carlo analysis of two-photon fluorescence imaging through a scattering medium," *Appl. Opt.* **37**, 8092–8102 (1998).
26. A. K. Dunn, V. P. Wallace, M. Coleno, M. W. Berns, and B. Tromberg, "Influence of optical properties on two-photon fluorescence imaging in turbid samples," *Appl. Opt.* **39**, 1194–1201 (2000).
27. X. Deng, X. Gan, and M. Gu, "Multiphoton fluorescence microscopic imaging through double-layer turbid media," *J. Appl. Phys.* **91**, 4659–4665 (2002).
28. X. Deng, X. Gan, and M. Gu, "Monte Carlo simulation of multiphoton fluorescence microscopic imaging through inhomogeneous tissue like turbid media," *J. Biomed. Opt.* **8**, 440–449 (2003).
29. X. Gan and M. Gu, "Fluorescence microscopic imaging through tissue-like turbid media," *J. Appl. Phys.* **87**, 3214–3221 (2000).
30. L. Moreaux, O. Sandre, and J. Mertz, "Membrane imaging by second-harmonic generation microscopy," *J. Opt. Soc. Am. B* **17**, 1685–1694 (2000).
31. C. F. Bohren and D. R. Huffman, *Absorption and Scattering of Light by Small Particles*, Wiley, New York (1983).
32. X. Deng and M. Gu, "Penetration depth of single-, two- and three-photon fluorescence microscopic imaging through human cortex structures: Monte Carlo simulation," *Appl. Opt.* **42**, 3321–3329 (2003).